Effect of the hydroxamate group in the antitumoral activity and toxicity toward normal cells of new copper(II) complexes

Nathália F. B. Azeredo · Franz V. Borges · Marcelo S. Mathias ·
Jackson A. L. C. Resende · Roberto W. A. Franco · Milton M. Kanashiro ·
Adolfo Horn Jr. · Christiane Fernandes

Abstract The synthesis, physico–chemical characterization and cytotoxicity of four copper(II) coordination complexes, i.e. $[Cu(HBPA)Cl_2]$ (1), $[Cu(BHA)_2]$ (2), $[Cu(HBPA)(BHA)Cl]$ CH_3OH (3) and $[Cu(HBPA)_2]Cl_2 \cdot 4H_2O$ (4), are reported. HBPA is the tridentate ligand N-(2-hydroxybenzyl)-N-(2-pyridylmethyl)amine and HBHA is the benzohydroxamic acid. The reaction between the HBHA and $CuCl_2 \cdot 2H_2O$ has resulted in the new complex (2) and the reaction between complex (1) and HBHA has resulted in the new complex (3). X-ray diffraction studies for complex (3) indicated the effective coordination of HBHA as BHA^-. Their cytotoxicity was evaluated against three human tumoral cell lines (Colo-205, NCI-H460 and U937) and PBMC (peripheral blood mononuclear cells), using the MTT cytotoxic assay. The results toward PBMC reveal that the new copper(II) complex (2) presents lower toxicity toward normal cells. Furthermore, complex (2) presents IC_{50} values lower than cisplatin toward NCI-H460 and the best selectivity index obtained towards NCI-H460 (SI = 2.2) and U937 cell lines (SI = 2.0), as a result of the presence of two molecules of HBHA

N. F. B. Azeredo · M. S. Mathias
Laboratório de Ciências Químicas, Universidade Estadual do Norte Fluminense, Campos dos Goytacazes, RJ 28013-602, Brazil

F. V. Borges
Instituto Federal Fluminense, Campos dos Goytacazes, RJ 28030-130, Brazil

J. A. L. C. Resende
Instituto de Ciências Exatas e da Terra, Campus Universitário do Araguaia, Universidade Federal de Mato Grosso (UFMT), Barra do Garças, MT, Brazil

R. W. A. Franco
Laboratório de Ciências Físicas, Universidade Estadual do Norte Fluminense, Campos dos Goytacazes, RJ 28013-602, Brazil

M. M. Kanashiro
Laboratório de Biologia do Reconhecer, Universidade Estadual do Norte Fluminense Darcy Ribeiro, Campos dos Goytacazes, RJ 28013-602, Brazil

A. Horn Jr. · C. Fernandes (✉)
Departamento de Química, Universidade Federal de Santa Catarina, Florianópolis, SC 88040-900, Brazil
e-mail: christiane.horn@ufsc.br

in its structure. Complex (3) presents IC$_{50}$ values lower than cisplatin toward NCI-H460, Colo-205 and comparable to cisplatin toward U937. The evaluation of the cell death type promoted by complexes (2) and (4) was investigated toward NCI-H460 revealing better results than the standard drug cisplatin, according to the Annexin V and propidium iodide (PI) labeling experiment. Based on the studies here performed, HBHA seems to be related to lower toxicity toward PBMC and HBPA is improving directly the cytotoxity.

Introduction

Hydroxamic acids, both origin natural and synthetic, are a class of organic complexes extensively studied with a variety of applications (Končić et al. 2011; Gupta and Sharma 2013; Marmion et al. 2013; Rodrigues et al. 2016; Wang et al. 2018). In recent years, hydroxamic acid derivatives have attracted the attention due to their potential in combating various etiological factors associated with cancer (Luu et al. 2008; Saban and Bujak 2009; Kovacic and Edwards 2011; Kenny et al. 2020). The first hydroxamic acid approved by the FDA to enter clinics as a treatment of cutaneous T-cell lymphoma (Codd et al. 2009) was the suberoylanilide hydroxamic acid (SAHA) (Marks 2007) and it´s activity is associated with the inhibition of histone deacetylases (HDACs), including all 11 known human class I and class II HDACs. HDACs have many protein targets whose structures and functions are altered by acetylation, including histones and non-histones proteins components of transcription factors, which control gene expression and proteins that regulate cell proliferation, migration and death (Kim et al. 2003; Parker et al. 2013). The mechanism involved in SAHA cytotoxicity effects was identified as inhibition of the histone deacetylases (HDACs), a finding based on recognition of the similarity of SAHA structure to the trichostatin A (Parker et al. 2013; Halaburková et al. 2017). Its antitumor activity is also associated to multiple mechanisms, including cell cycle arrest, intrinsic and extrinsic apoptosis,

generation of reactive oxygen species (ROS) and inhibition of angiogenesis, both *in vitro* and *in vivo*. This compound is well tolerated by patients in doses with potent antitumor activity (Park et al. 2015).

Marmion and coworkers have been developing platinum metal complexes containing hydroxamic acids, obtaining new molecules with a platinum(II) center at one side of the molecule and a hydroxamic acid at the other (Griffith et al. 2011a; Brabec et al. 2012; Parker et al. 2013). This strategy resulted in molecules with increased and more selective antitumor activities compared to their starting reagents (Griffith et al. 2011b). The *in vitro* study of the cis-[Pt(NH$_3$)$_2$(Mal-p-Bel-2H)] complex revealed that it has (i) substantial cytotoxicity against ovary cancer cell lines, (ii) increased cytotoxicity over the previous platinum compound reported (*cis*-[Pt^{II}(NH$_3$)$_2$(-malSAHA$_{-2H}$)]), and (iii) favorable cyto-selective properties compared to cisplatin and belinostat (Kenny and Marmion 2019).

A previous study using the histone deacetylase inhibitor SAHA decreased thioredoxin (Trx1) activity, due to the formation of complex with Trx1 and an increase of reactive oxygen species (ROS) formation. This study revealed that one possible mechanism for the anticancer effect of SAHA is via the Trx1 system and proves that SAHA induces an increase in Txnip protein levels that can bind and inhibit Trx1. Thus this would lead to a decreased oxidative stress defense, oxidation, as well as inhibit Trx1 binding to ASK1, thus promoting apoptosis (Ungerstedt et al. 2012). *In vivo* studies demonstrated that SAHA decreases viability and increases apoptosis similarly to the paclitaxel for ovarian cancer chemotherapy (Cooper et al. 2007).

Great efforts are currently underway for the design of better prototypes for the treatment of cancer, as well as other robust applications in health care, based on the hydroxamic acids (Manal et al. 2016; Wang et al. 2018). In this sense, we report herein the synthesis, characterization and antitumoral activity of two new copper(II) complexes [Cu(HBHA)$_2$] (2) and [Cu(HBPA)(HBHA)Cl] CH$_3$OH (3), both coordinated to the benzohydroxamic acid (HBHA), with relevant antitumor activities. The goal of this work is to obtain complexes less toxic to normal cells and with a higher capacity to overcome some undesirable side effects, as well as the acquired resistance, common in cisplatin treatments. In order to achieve this goal we observed

that the reactions between hydroxamic acids and the copper(II) complexes are favored by the chelate effect and by the presence of labile ligands such as chloride in the structures of the complexes, leading to the formation of stable hydroxamate complexes. Therefore, complex **(1)**, previously reported by us (Borges et al. 2016), was selected to this investigation. This complex induced apoptotic cell death by activating both the intrinsic and extrinsic pathways. *In vivo* results revealed that complex **(1)** was effective against human acute monocytic leukemia (THP-1) and murine melanoma cells lines (B16-F10). BALB/c nude bearing THP-1 tumors treated with 12 mg kg^{-1} of this complex showed a 92.4% inhibition of tumor growth compared to the control group (Borges et al. 2016).

Here we are also going to evaluate the type of death promoted by the most promising complexes in tumor cells through annexin-V and propidium iodide (PI) labeling studies. The comparison of cytotoxic activity of these complexes with the respective ones without hydroxamic acid, against the same cell lines, will be presented.

Experimental

General

Reagents and solvents were used as received from commercial sources. The ligands and their respective copper(II) complexes were synthesized using analytical grade reagents. The elemental analysis (CHN) for the complexes was performed with a Perkin Elmer 2400 CHN analyzer. The determination of melting point (MP) was carried out employing a Microquimica MQAPF-301 apparatus. Infrared spectras were recorded with a Shimadzu FT-IR 8300 spectrophotometer. The solid samples were prepared in a KBr pellet and the spectra recorded over the frequency range of 400–4000 cm^{-1}. UV–Vis spectras were recorded with a UV–Vis Varian, Cary 50 Bio, using DMF (dimethylformamide) as solvent. Full scan mass spectra (MS mode) were obtained with a MicroTOF LC Bruker Daltonics spectrometer equipped with an electrospray source operating in positive ion mode. Samples were dissolved in a MeOH/H$_2$O (50/50) solution and were injected in the apparatus by direct infusion. The electrical conductivity of solution of each complex (1 × 10^{-3} mol L^{-1}) was measured

with a Biocristal conductometer in DMF. X-ray diffraction data was carried out with a Bruker D8-Venture diffractometer equipped with the detector Photon 100 CMOS using microfocus MoKα (λ = 0,71,073 Å) X-ray radiation at 150 K. The crystal data was collected using APEX2 (BRUKER 2012). The structure was solved and refined with SHELX package (Sheldrick 2008). Electron Paramagnetic Resonance (EPR) spectra were obtained using a Bruker E500 spectrometer using a highly sensitive cylindrical cavity, operating in X-band (9 GHz), at 100 K, with 5 mW microwave power, 5 G modulation amplitude and 100 kHz modulation frequency. The spectra were simulated using the Qpow program (Maurice 1980) and a MgO:Cr(III) (g = 1.9797) marker.

Synthesis

The ligand HBPA was synthesized as previously described (Neves et al. 1993). HBPA has been used as a ligand and a precursor of the ligand (N-(2-hydroxybenzyl)-N-(2-pyridylmethyl)[(3-chloro)(2-hydroxy)]propylamine]) (H$_2$BPClNOL), which has been extensively studied by us (Silva et al. 2008; Fernandes et al. 2010, 2014; Costa et al. 2018). Scheme 1 shows the synthesis of complexes **(1)**–**(4)**.

[Cu(HBPA)Cl$_2$] **(1)**. Complex **(1)** was synthesized according to the methodology previously described in literature (Borges et al. 2016). Yield: (430 mg) 82%. Elemental anal. found (%): C = 41.87; H = 4.18; N = 7.56. Calcd. for CuC$_{13}$H$_{16}$N$_2$O$_2$Cl$_2$ (%) = C = 41.56; H = 4.56; N = 7.46. MP: 170 °C (18 μS cm^{-1} non-electrolyte type). (Geary 1971).

[Cu(BHA)$_2$] **(2)**. Complex **(2)** was obtained by reacting 2 mmol (274 mg) of HBHA and stoichiometric amounts of KOH (1 mmol, 56 mg) and copper(II) chloride salt dehydrate (1 mmol, 170.5 mg), in 20 mL of methanol, under reflux. After 30 min of reaction a thin, moss–green amorphous solid was obtained, which was filtrated and dried under vacuo. Yield: (306 mg) 41%. Elemental anal. found (%): C = 48.97; H = 3.0; N = 8.49. Calcd. for CuC$_{14}$H$_{12}$N$_2$O$_4$ (%) = C = 50.07; H = 3.6; N = 8.34. IR cm^{-1}: 3420 (ν NH), 3190-2710 (ν OH), 3050 (ν CH$_{Aromatic}$), 2957, 2915, 2868 and 2812 (ν CH$_2$ and ν CH$_3$), 1605, 1587, 1524 and 1489 (ν C = C and ν C = N), 791, 685, 469 and 424 (γ-CH aromatic and β-

Scheme 1 Synthesis of the new copper(II) complexes containing HBHA ((**2**) and (**3**)) and the complexes previously reported ((**1**) and (**4**)) (Azeredo et al. 2015; Borges et al. 2016)
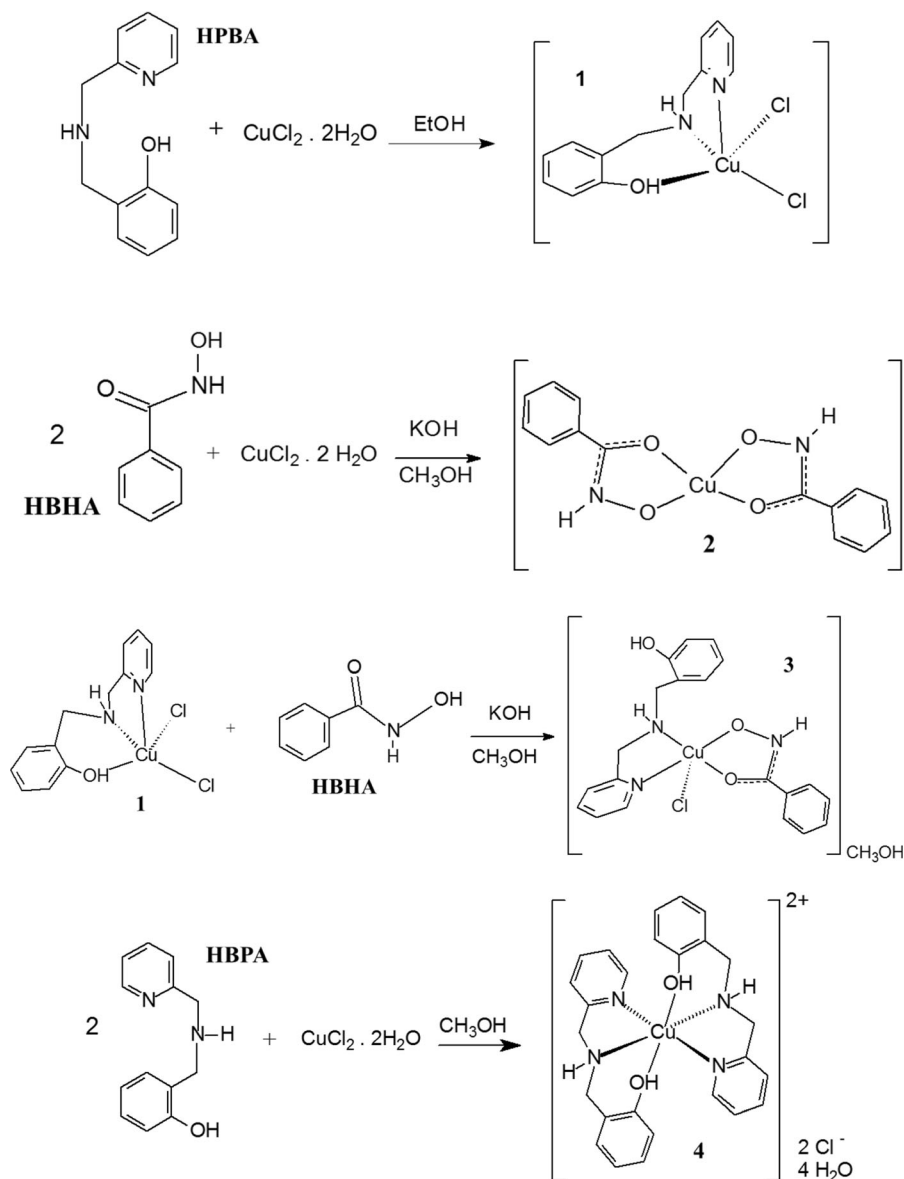
ring aromatic). MP: 205 °C (4 µS cm^{-1} non-electrolyte type). (Geary 1971).

[Cu(HBPA)(BHA)Cl] CH$_3$OH (**3**). Complex (**3**) was obtained by reacting 1 mmol of BHA (137 mg) and 1 mmol of complex (**1**) (348 mg). Initially, HBHA was deprotonated with a stoichiometric amount of KOH and then a methanolic solution of complex (**1**) was added to the solution containing deprotonated BHA$^-$. The reaction was conducted under reflux and dark green single crystals were obtained after a few days. Yield: (220 mg) 60%. Elemental anal. found (%): C = 52.2; H = 5.3;

N = 8.8. Calcd. for CuC$_{21}$H$_{25}$N$_3$O$_4$Cl (%): C = 52.3; H = 5.2; N = 8.7. IR cm^{-1}: 3500 (ν NH), 3200-2800 (ν OH), 1657, 1609, 1578, and 1514 (ν C = C and ν C = N), 1485, 1456, 1431 (ν CH$_2$ and ν CH$_3$) and 787, 750, 694, 670 (γ-CH aromatic and β-ring aromatic). MP: 150 °C (50 µS cm^{-1} non-electrolyte type). (Geary 1971).

[Cu(HBPA)$_2$]Cl$_2$.H$_2$O (**4**). Complex (**4**) was synthesized as previously described by Azeredo and coworkers (Azeredo et al. 2015). Yield: (270 mg) 86%. Elemental anal. found (%): C = 49.1; H = 5.8; N = 8.9. Calcd. for CuC$_{21}$H$_{25}$N$_3$O$_4$Cl (%):C = 49.2;

H = 5.7; N = 8.8. MP: 175 °C (130 µS cm^{-1} 2:1 electrolyte type). (Geary 1971).

Antitumor activity

Cell culture

Human leukemia cell line Colo-205 (human colon adenocarcinoma), NCI-H460 (lung carcinoma) and U937 (histiocytic lymphoma cell line) were cultured routinely in DMEM-F12 medium, (Dulbecco's Modified Eagle Medium) (Gibco, BRL) supplemented with 10% fetal calf serum and gentamicin (20 µg mL^{-1}, Gibco, BRL) and incubated at 37 °C in a humidified atmosphere containing 5% CO$_2$. Blood samples were collected from healthy donors in Sodium Heparin glass tubes "VacutainerTM" (Becton Dikinson) and the peripheral blood mononuclear cells (PBMC) isolated over Ficoll–Paque^{TM} Plus (1.08 g mL^{-1}) in a 50 mL conical tube (2:1—blood:ficoll). Twenty milliliters of fresh heparinized blood sample were diluted in phosphate buffer saline (PBS), gently laid over 10 mL of Ficoll and centrifugated at 1500 rpm for 40 min at 25 °C. PBMC rings were collected and washed three times with PBS by centrifugating at 1500 rpm for 10 min at 4 °C. After the washing process, the supernatant was discarded and the cells were suspended in DMEM-F12 medium supplemented with 10% fetal bovine serum, 20 µg ml^{-1} gentamicin and 0.25 µg ml^{-1} Staphilococcus enterotoxin B (Sigma, S0812). Trypan blue solution 0.4% (Sigma, Germany) was used to count the cells into an appropriate concentration and the viability of cells was checked. The required range of cells' viability was maintained between 95% and 99%. Stock solutions of synthesized complexes and cisplatin were prepared at a concentration of 0.02 mol L^{-1}, using dimethyl sulfoxide (DMSO) and water as solvents. Stock solutions were stored in a freezer to remain stable. The complexes previously dissolved in DMSO were diluted in DMEMF12 culture medium, (Gibco, BRL) supplemented with 20 mg mL^{-1} gentamicin (Gibco, BRL) and 10% fetal bovine serum (Gibco, BRL) to achieve the working concentrations (100 µmol L^{-1}, 50 µmol L^{-1}, 25 µmol L^{-1}, 12.5 µmol L^{-1} and 6.25 µmol L^{-1}).

Cell viability study

The cell viability assays were performed according to a previously described methodology (Mosmann 1983), by evaluating the MTT (3-(4,5-dimethyl- 2-thihazyl)-2,5-diphenyl-2H-tetrazolium bromide) (Sigma, M2128) metabolization. Tumoral and normal cells (Colo-205, NCI-H460, U937 and PBMC, respectively) were plated in 96-well plates at densities of 1×10^6 cells mL^{-1}, and different concentrations of the copper(II) complexes (100 µM, 50 µM, 25 µM, 12.5 µM and 6.5 µM) were added to the culture and maintained for 36 h at 37 °C. Twenty microliters of MTT stock solution (5 mg mL^{-1}) were added into each well, containing 100 µL of the tested compound, and the cells were incubated at 37 °C for 4 h with 5% of CO$_2$. After this period, 120 µL of the supernatant were removed and the formazan crystals were dissolved in 150 µL of acidic isopropanol. The 96-well plates were centrifuged to separate solid remains of cells debris, and a 100 µL aliquot from each well was transferred to a clean plate for spectrophotometric quantification at 570 nm wavelength. The absorbance was determined at 570 nm using a microplate reader, (Thermo Labsystems Multiskan, 352 model) and each concentration was evaluated in three independent experiments run in triplicate. Cisplatin (Sigma) was used as a positive control. The absorbance results obtained were converted to viable cell percentage and the IC$_{50}$ values were obtained using GraphPad Prism 5.0. The selectivity index (SI) was calculated as presented in Eq. 1 (Muller and Milton 2012).

$$SI = IC_{50}(PBMC) / IC_{50}(tumor\ cell) \qquad (1)$$

Evaluation of cell death pathway

To evaluate if the complexes induced necrosis or apoptosis 10^6 in the cells, experiments using flow cytometry (annexin V/propidium iodide staining) were carried out by. Tumoral cells were cultured at 2×10^6 cells mL^{-1} for non-adherent strains (U937) and $1 \times$ cells mL^{-1} for adherent strains (Colo-205 and NCI-H460), in 24 multiwell plates. After 4-6 h (37 °C with 5% CO$_2$), the cells were treated with 1 mL of the copper(II) complexes at a final concentration of $1 \times IC_{50}$ and $2 \times IC_{50}$ for 24 h, 36 h or 48 h (depending on the compound). Briefly, after

incubation, the cells were washed twice with PBS and incubated in 500 μL of binding buffer (100 mM HEPES/NaOH, pH 7.5, 1.4 M NaCl and 25 mM CaCl₂). 5 μL of Annexin V-FITC (Sigma–Aldrich) and 10 μL of PI (Sigma–Aldrich) were added to each sample. They were then incubated at room temperature for 10 min protected from light. Cell fluorescence was determined immediately with a flow cytometer (FACS Calibur-BD). The result was determined by recording 10.000 events per sample (Rieger et al. 2011).

Results and discussion

Among the four complexes described in this work, the synthesis and molecular structures of complexes (1) and (4) were previously reported by us (Azeredo et al. 2015) (Borges et al. 2016) We have previously described the antitumor activity of (1) *in vitro* and *in vivo* as well (Borges et al. 2016). While complex (1) contains only one molecule of the ligand HBPA, complex (4) contains two of them. In addition, we have observed that ligands derived from the HBPA generate complexes with expressive antineoplastic activities (Fernandes et al. 2015; Morcelli et al. 2016; Moreira et al. 2019; Maciel et al. 2020) Furthermore, complexes containing hydroxamic acid derivatives have also shown antitumor activity (Kenny and Marmion 2019; Kenny et al. 2020). Aiming to develop new anticancer agents with better activity, we decided to study the formation of a new heteroleptic copper(II) complex containing the ligands HBPA and HBHA (HBPA is the tridentate ligand N-(2-hydroxybenzyl)-N-(2-pyridylmethyl)amine and HBHA is the benzohydroxamic acid). In this sense, the four complexes presented in Scheme 1 were tested against three different cancer cell lines. The only complex isolated as an amorphous solid was [Cu(HBHA)₂], however it´s characterization data obtained agree with the formation of a mononuclear copper(II) complex.

X-ray molecular structure

The single crystal X-ray data obtained for complex (3) reveals the formation of a pentacoordinated copper(II) complex containing a benzohydroxamate anion (BHA⁻), a molecule of HBPA ligand and a chlorine. A methanol molecule is present as the solvent of crystallization, resulting in an empirical formula of $CuC_{21}H_{24}ClN_3O_4$ and a molecular weight of 481.42 g mol⁻¹.

The geometry presented by complex (3) is described as a near ideal square pyramidal, with an Addison parameter (τ) value of 0.05 (Addison et al. 1984). The benzohydroxamate anion is coordinated in a bidentate manner to the metallic center (through alcohol and carbonyl oxygen atoms) and, together with the ligand HBPA, form the base of the pyramid, which contains a chloro ligand in the apical position (Fig. 1). The most relevant bond lengths and angles are shown in Table 1 and crystallographic data for complex (3) are presented in Table 2. It is important to highlight that the coordination behavior of ligand HBPA in (3) differs from the observed in complexes (1) and (4). While in complex (1) the HBPA ligand shows a tridentate coordination mode and the phenol group interacts with the copper center in the protonated form, in (3), the phenol group is not coordinated to the metal center. Due to this arrangement, the HBPA ligand shows a bidentate coordination mode in (3). Similar behavior for the phenol group was found in the zinc(II) complex [Zn(HBPA)Cl₂], previously reported by us (Fernandes et al. 2014).

The distance between the metallic center and the pyridine nitrogen (N20) of 1.987(5)Å, is similar to the distance between the metallic center the amine nitrogen (N1) of 2.012(5)Å. This similarity suggests that the pyridine and the amino groups have similar basicity. On the other hand, the bonds formed between BHA⁻ and the copper(II) anion (Cu1–O2A and Cu1–O1A) are shorter, suggesting that the amine and pyridine groups have less affinity for the metallic center than the oxygen from the alkoxide and carbonyl groups present in the benzohydroxamate ligand (HBHA). The longest distance is observed in the Cu1–Cl1 bond [(2.679(2)Å].

ESI-(+)-MS

Data of ESI-(+)-MS spectra will be presented for the complexes (2), (3) and (4). Data for complex (1) were reported previously (Borges et al. 2016). The spectra and the structures proposal were based on the isotopic patterns for the main ions of each complex and are presented in the Supplementary Material (S1-S15).

The ESI-(+)-MS spectrum of complex (2) (Fig. S1) shows an intense signal of *m/z* 336 attributed
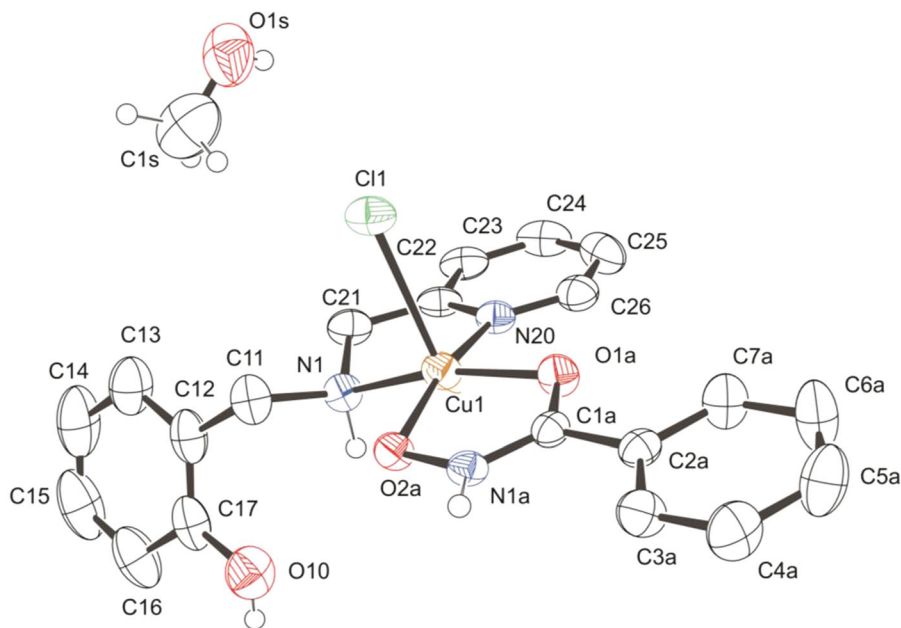
Fig. 1 X-ray structure of complex (**3**)

Table 1 The main bond lengths and angles in complex (**3**)

Atoms	Distances/Å
Cu(1)–Cl(1)	2.6790(14)
Cu(1)–N(1)	2.012(5)
Cu(1)–N(20)	1.987(5)
Cu(1)–O(1A)	1.951(4)
Cu(1)–O(2A)	1.935(4)
	Angles/°
O(2A)–Cu(1)–N(20)	168.31(19)
O(1A)–Cu(1)–N(1)	165.15(18)
N(20)–Cu(1)–Cl(1)	98.37(14)
O(1A)–Cu(1)–Cl(1)	97.90(13)
N(1)–Cu(1)–Cl(1)	96.89(15)
O(2A)–Cu(1)–N(1)	96.27(18)
O(1A)–Cu(1)–N(20)	94.33(19)
O(2A)–Cu(1)–Cl(1)	93.31(12)
O(2A)–Cu(1)–O(1A)	84.24(18)
N(20)–Cu(1)–N(1)	82.2(2)

to the cation of the compound in which one HBHA ligand is in protonated form (HBPA) and the other, BHA$^-$ is in deprotonated form, resulting in: [Cu(HBHA)(BHA)]$^+$. The most intense signal in the spectrum (m/z 358) is assigned to the cation Na[Cu(BHA)$_2$]$^+$. The signals of m/z 534, m/z 734 and m/z 932 refer to the dimers, trimers and tetramers of the original complex where the copper center shows reduced oxidation state ([Cu$^I_2$(BHA)(HBHA)$_2$]$^+$, [Cu$^I_3$(BHA)$_2$(HBHA)$_2$]$^+$ and [Cu$^I_4$(BHA)$_5$]$^+$). These species are possibly formed in gas–phase after ionization. The MS/MS analysis of the signal of m/z 932 reveals that this ion forms the species of m/z 534 ([Cu$^I_2$(BHA)(HBHA)$_2$]$^+$), 358 (Na[Cu(BHA)$_2$]$^+$) and 336 ([Cu(HBHA)(BHA)]$^+$) (Figs. S2–S5).

The ESI-(+)-MS spectrum obtained of complex (**3**) (Fig. S6) shows the most intense peak at m/z 413, attributed to the cation [Cu(HBPA)(BHA)]$^+$, confirming the formation of a mononuclear copper(II) complex in solution and the coordination of the benzohydroxamic acid (HBHA) in the deprotonated form. Another signal with copper profile is present with m/z 589, whose proposal indicates a binuclear complex [(HBPA)Cu^I(μ-Cl)Cu^I(HBPA)]$^+$. It is also possible to visualize the signal of ligand HBPA in its protonated form [H$_2$BPA]$^+$, with m/z 215. Another signal observed in the spectrum of m/z 276 is equivalent to a copper(II) center coordinated only to the ligand HBPA: [Cu(HBPA)]$^+$. The MS/MS study of the signal of m/z 413 reveals that this ion gives rise to the cations of m/z 276 ([Cu(HBPA)]$^+$) and 215

Table 2 Crystal data and structure refinement for complex (3)

Empirical formula	$C_{21}H_{24}ClCuN_3O_4$
Formula weight	481.42
Temperature/K	291.01
Crystal system	Triclinic
Space group	P1
a/Å	6.4321(4)
b/Å	6.8547(4)
c/Å	12.4876(8)
α/°	98.612(3)
β/°	94.805(3)
γ/°	101.884(3)
Volume/Å^3	528.95(6)
Z	1
ρ_{calc}g/cm^3	1.511
μ/mm^{-1}	1.192
F(000)	249.0
Crystal size/mm^3	0.276 × 0.085 × 0.065
Radiation	MoKα (λ = 0.71073)
2Θ range for data collection/°	6.484 to 52.174
Index ranges	$-7 \leq h \leq 7$, $-8 \leq k \leq 8$, $-15 \leq l \leq 15$
Reflections collected	9385
Independent reflections	4123 [R_{int} = 0.0363, R_{sigma} = 0.0468]
Data/restraints/parameters	4123/3/275
Goodness-of-fit on F^2	1.073
Final R indexes [I > = 2σ (I)]	R_1 = 0.0379, wR_2 = 0.0782
Final R indexes [all data]	R_1 = 0.0469, wR_2 = 0.0828
Largest diff. peak/hole / e Å^{-3}	0.27/−0.43
Flack parameter	−0.023(18)

([H$_2$BPA]$^+$). All fragments present in the spectrum were assigned based on their isotopic profiles (Figs. S7–S10).

The ESI-(+)-MS spectrum of complex (4) (Fig. S11) reveals three intense cationic species with copper profile (m/z 276, m/z 490 and m/z 589). The protonated HBPA ligand signal is observed at m/z 215 [H$_2$BPA]$^+$ and the signal of m/z 276 is assigned to the equivalent copper(II) center coordinated to the deprotonated form of the HBPA ligand, resulting in the cation [Cu(HBPA)]$^+$. This was also observed in the ESI-(+)-MS spectrum of complex (3) (Figs. S12–S13). The signal of m/z 490 corresponds to the cation containing two units of the ligand HBPA, one of them is in anionic form, resulting in the species [Cu(HBPA)(BPA)]$^+$ (Fig. S14). The peak at m/z 589 was attributed to a binuclear species [(HBPA)Cu^I(μ–Cl)Cu^I(HBPA)]$^+$ (Fig. S15).

Infrared and electronic spectra

The infrared spectrum of complex (2) (Fig. S16) shows more defined bands and variations in the wave number in comparison to the ligand HBHA spectrum. The characteristic hydroxyl band is narrower/straighter in the complex (2) spectrum when compared to the OH vibration in HBHA spectrum, showing the effective action of potassium hydroxide (KOH) in deprotonating the hydrogen from alcohol and proving the coordination of copper(II) to the oxygen atom. The appearance of a shoulder at 3420 cm^{-1}, characteristic of the associated NH stretch in secondary amines is also observed in complex (2). In the HBHA spectrum, this band is overlapped due to the broad band of the hydroxyl group.
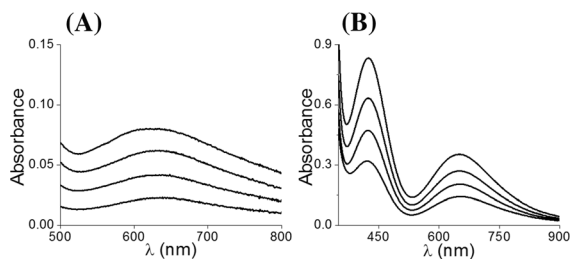
The infrared spectrum of complex (3) (Fig. S17) shows the characteristic bands of the HBHA ligand

and the precursor copper(II) complex (1), such as the OH vibration in the region between 3200 cm^{-1} and 2800 cm^{-1} and the axial deformation of CO and CN present between 1354 cm^{-1} and 1244 cm^{-1}. The presence of axial deformation of C = C of aromatics in 1657 cm^{-1} and 1609 cm^{-1} is also observed. The angular deformation bands of the aromatic ring replaced are found in 787 cm^{-1}, 750 cm^{-1}, 694 cm^{-1} and 670 cm^{-1}.

The spectrum in the infrared region obtained for complex (4) was compared to the HBPA ligand in the region between 4000 cm^{-1} and 400 cm^{-1} (Neves et al. 1993). Bands characteristic of the aromatic groups are observed in complex (4) between 1612 cm^{-1} and 1433 cm^{-1} (νC = C and νC = N), at 3345 cm^{-1} for the stretch of the νNH bond, and at 1365 cm^{-1} due to the phenol group (δOH). These results (Fig. S18) are in agreement with those previously published by us for HBPA (Azeredo et al. 2015). The bands present in the large region between 3500 cm^{-1} and 3100 cm^{-1} in complex (4) are attributed to the overlapping of the hydroxyl group (OH) of phenol, the axial deformations of the aromatic C–H in 3041 cm^{-1} and 3009 cm^{-1} and the aliphatic C–H in 2947 cm^{-1} and 2858 cm^{-1}. The phenol C–O stretch band appears at 1272 cm^{-1}. The displacement of the bands to regions of different wavenumbers, in comparison to the ligand infrared spectrum, shows the weakening of some bonds and changes in the geometry, confirming the complexation and the obtainment of complex (4) (Azeredo et al. 2015).

The electronic spectra of the new complexes (2) and (3) were obtained in DMF and are presented in Fig. 2a and b, respectively. Complex (2) presents a low intensity d–d transition at 634 nm (48.3 L mol^{-1} cm^{-1}). Complex (3) presents a band at 423 nm (400 L mol^{-1} cm^{-1}), with an ε value a slightly higher than a typical d–d, and also a d–d transition at 648 nm (140 L mol^{-1} cm^{-1}). In agreement with previous studies carried out for complex (4) (Azeredo et al. 2015), we can state that the high ε value observed for the band at 423 nm is indicating the partial deprotonation of the phenol groups and its coordination to the copper center as a phenolate. Complex (4) exhibits two transitions in DMF, at 429 (341 dm^3 mol^{-1} cm^{-1}) and at 661 nm (163 dm^3 mol^{-1} cm^{-1}) previously attributed to phenolate pπCu^{2+} dσ^* charge transfer (LMCT) and d–d transition, respectively (Azeredo et al. 2015).

Electrochemical studies

The electrical conductivity measurement performed for all the new complexes shows their poor ionizable nature (neutral complexes). The values observed for complexes (2) (4 µS cm^{-1}) and (3) (50 µS cm^{-1}) were below 65 µS cm^{-1} (non-electrolyte complex formation in solution), suggesting that the solid state structures were kept in solution. Although complex (3) presents a long–distance Cu–Cl, based on the X-ray diffraction studies, and some dissociation in solution is expected, its low value conductivity proves a non-electrolyte complex.

Compound (2) was not soluble in the concentration required to observe any redox process related to the copper oxidation/reduction by cyclic voltammetry. The cyclic voltammogram of complex (3) shows the presence of two cathodic and two anodic redox processes. The cathodic processes were observed at
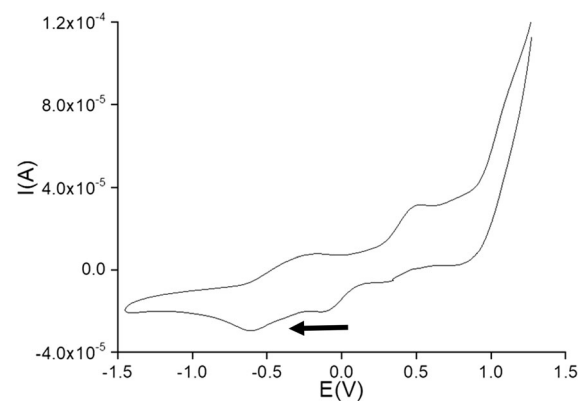

Fig. 2 Electronic spectra in DMF of the complexes (a) (2), in the concentrations 0.2–1.4 × 10^{-3} mol L^{-1} (b) (3), in the concentrations 1.0–2.5 × 10^{-3} mol L^{-1}

Fig. 3 Cyclic voltammogram of the complex (3). Working electrode: glassy carbon; pseudo-reference electrode: platinum; counter electrode: platinum; supporting electrolyte: tetrabutylammonium perchlorate 0.1 mol dm^{-3}; solvent DMF

−0.168 V and −0.327 V vs NHE, while the anodic processes at 0.037 V and 0.784 V vs NHE (Fig. 3).

The presence of only one redox process would be expected, since complex (3) is a mononuclear species. The presence of a large number of such processes can be attributed to the formation of more than one species in solution. For example, the chloro ligand is labile and can be replaced in some extension by solvent molecules. This can be also induced by the reduction process, since Cu(I) prefers a tetracoordinated environment than a pentacoordinated one. According to X-ray diffraction data, complex (3) is a mononuclear copper(II) complex, containing both ligands HBPA and HBHA coordinated. However, in solution, this complex undergoes changes in the coordination sphere, suggesting the occurrence of a coupled reaction (chloride ligand release, phenol coordination and/or interaction with solvent molecules), generating two distinct species that are in equilibrium (Azeredo et al. 2015).

EPR spectroscopy

Figure 4 shows the EPR spectra of the complexes (1)–(4). All spectra are characteristic of Cu(II) in an axial site. The Cu(II) has $3d^9$ electronic configuration, electron spin S = 1/2 and nuclear spin I = 3/2 and, therefore, the hyperfine interaction between electron and nucleus produces four lines (2*I + 1 = 4). For an axial site, a set of four parallel and four perpendicular signals are expected. The spectra were simulated considering electronic Zeeman and hyperfine interactions, and the parameters obtained from simulations are listed in Table 3. The spectrum of complex (1) was simulated considering just one Cu(II) site (S1). However the simulated spectra for complexes (2), (3) and (4) represent the sum of two spectra, and each one is associated to one Cu(II) site: (S21 and S22) for complex (2), (S31 and S32) for complex (3) and (S41 and S42) for complex (4) (Fig. 4). The relative intensity of each Cu(II) site, showed in Table 3, was obtained by double integration of each simulated spectrum. All simulated spectra show $g_{//} > g_{\perp-} > 2.0023$ and $A_{//} > A_{\perp}$, which are characteristic of Cu(II) in an elongated octahedral site and ground state $d_{x^2-y^2}$ (Kalfaolu and Karabulut 2011).

The $g_{//}$ value is related to the nature of copper environment (Kivelson and Neman 1961), so that the $g_{//} < 2.3$ indicates the covalent interaction between
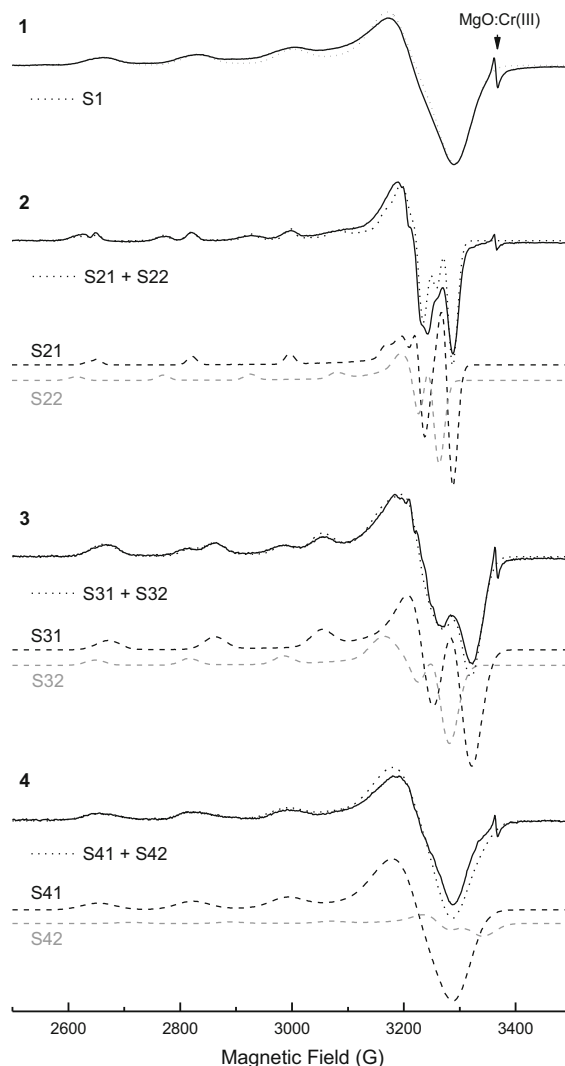
Fig. 4 EPR spectra of complexes (1)–(4) (solid lines) and its simulations (dotted lines). The simulations for the spectra presented for complexes (2), (3) and (4) are represented by the sum of two spectra (dashed lines): (S21 and S22) for complex (2), (S31 and S32) for complex (3) and (S41 and S42) for complex (4). MgO:Cr(III) was used as g-factor reference

Cu(II) and its ligands. This is the case of all spectra of complexes (1), (3) and (4), which have the ligand HBPA coordinated to the Cu(II) centers. For complex (2), the S21 site has $g_{//} < 2.3$ and S22 site has $g_{//} > 2.3$, which indicates the ionic environment, as effect of the coordination of two ligands HBHA to the copper(II).

The G parameter, defined as $G = (g_{//} - 2.0023)/(g_{\perp} - 2.0023)$, is an indication for the exchange

Table 3 EPR parameters of complexes (**1**)–(**4**)

Compound	Cu(II) site	Relative intensity (%)	$g_{//}$	$g_{\perp}$	$A_{//}$ (MHz)	$A_{\perp}$ (MHz)	$g_{//}/A_{//}$ (cm)	G
(**1**)	S1	100	2.271 ± 0.001	2.062 ± 0.003	530 ± 10	46 ± 5	129	4.501
(**2**)	S21	53	2.29 ± 0.005	2.065 ± 0.005	550 ± 5	30 ± 10	125	4.589
	S22	47	2.34 ± 0.005	2.07 ± 0.01	500 ± 5	25 ± 10	140	4.99
(**3**)	S31	66	2.253 ± 0.001	2.06 ± 0.005	590 ± 10	25 ± 5	115	4.35
	S32	34	2.297 ± 0.001	2.07 ± 0.005	530 ± 10	50 ± 5	130	4.35
(**4**)	S41	90	2.292 ± 0.001	2.063 ± 0.005	530 ± 10	30 ± 5	130	4.773
	S42	10	2.235 ± 0.005	2.04 ± 0.01	550 ± 10	10 ± 5	122	6.17

interactions between Cu(II) centers (Hathaway and Billing 1970). For the spectra of all complexes, $G > 4$ was obtained, which is characteristic of the exchange interaction negligible, and therefore, no spin–exchange interaction between Cu(II) exists in the analyzed samples.

The ratio $g_{//}/A_{//}$, in cm, is an index of tetrahedral distortion of Cu(II) sites (Faggi et al. 2015). All spectra of complexes (**1**), (**3**) and (**4**) have ratio $g_{//}/A_{//}$ values within the range from 105 cm to 135 cm, which corresponds to the square planar arrangement of atoms in the equatorial plane. The same arrangement is observed in the S21 site of the complex (**2**). For the S22 site, the ratio is 140 cm, which is out of range (150–250 cm), typical of tetragonal distortion sites. Therefore, this site shows a very small distortion in the equatorial plane.

All sites present in complexes (**1**), (**3**) and (**4**), which have at least one HBPA ligand coordinated to the Cu(II) centers, have square planar arrangement of atoms in the equatorial plane and covalent interaction between Cu(II) and its ligands. The EPR parameters of the new complex (**3**) is consistent with its geometry, determined by X-ray diffraction. Complex (**2**) is the only compound with two Cu(II) sites, similar relative intensities and different characteristic: the S21 site has a covalent environment and square planar arrangement at equatorial plane; the S22 site has an ionic environment and small distortion of equatorial plane.

Antitumoral activity evaluation

Evaluation of cell viability by MTT metabolization

The cytotoxicity against cancer cell lines (Colo-205, NCI-H460 and U937) were determined by means of the colorimetric MTT assay and the IC_{50} values were calculated in order to identify the more cytotoxic complexes, before carrying out studies related to cell death mechanism. The complexes were also tested towards normal cells (PBMC) and the selectivity index (SI) was calculated for *in-vitro* evaluations of the antiproliferative effect on normal tissues. Cisplatin, the prototype of many metal–based drugs, was also evaluated and included as a control drug. The IC_{50} values were determined based on the concentration dependence of viable cells 36 h after exposure to the complexes. The cytotoxic effect of the ligands HBPA and HBHA was also investigated.

Neither the ligand HBPA nor HBHA were cytotoxic to the tested cells up to a concentration of 100 µmol L^{-1} (Table 4). On the other hand, their complexation with copper (II) resulted in complexes with increased cytotoxicity. The best cytotoxic activity was observed for compound (**4**), which showed IC_{50} values in the range 20–30 µM for all the cancer cells. Cisplatin showed activity (20 ± 0.4 µM) only on the leukemia cell line tested (U937). The drawback for complex (**4**) is the high cytotoxicity levels it showed on the normal cell tested (PBMC).

Complex (**1**), which contains just one HBPA ligand, reduced cytotoxicity in lung cancer cells (NCI-H460) only. A better activity was shown by complex (**2**), which has two HBHA ligands. It was active on lung (NCI-H460) and leukemia (U-937) cell lines. Complex (**2**) also showed the lowest cytotoxicity against the normal cell (PBMC): 82 ± 0.4 µM. (Table 4) It was not active against Colo-205.

Complex (**2**) presents IC_{50} values lower than cisplatin toward NCI-H460 (38 ± 0.5 and > 200 µM, respectively) and the best selectivity index obtained towards NCI-H460 (SI = 2.2) and U937 cell lines (SI = 2.0), as a result of the presence of two molecules of HBHA in its structure. Complex (**3**), which contains

Table 4 IC$_{50}$ (μM) values obtained for the complexes by MTT metabolization assay

COMPOUNDS	Cell line			
	Colo-205[#]	NCI-H460[#]	U-937[#]	PBMC[#]
(1)	> 250[14]	56 ± 0.1	> 400[14]	45[14]
(2)	> 100	38 ± 0.5	42 ± 0.5	82 ± 0.4
(3)	35 ± 0.2	32 ± 0.2	31 ± 0.9	36 ± 0.1
(4)	20 ± 0.8	25 ± 0.9	27 ± 0.1	18 ± 0.5
HBPA	> 100[14]	> 100	> 150[14]	> 200[14]
HBHA	> 100	> 100	> 100	> 100
Cisplatin	> 100	> 200	20 ± 0.4	> 100
CuCl$_2$·2H$_2$O	> 200	> 200	> 200	–

[#]*Colo-205* bowel colon cancer, *NCI-H460* lung carcinoma, *U-937* human monocyte lymphoma, *PBMC* peripheral blood mononuclear cells

both ligands (HBPA and HBHA) on its structure, presents IC$_{50}$ values lower than cisplatin toward NCI-H460 (32 ± 0.2 and > 200 μM, respectively), Colo-205 (35 ± 0.2 μM and > 100 μM, respectively) and comparable to cisplatin towards U937 (31 ± 0.9 μM and 20 ± 0.4 μM, respectively). Complex (3) is more cytotoxic than complex (2), exhibiting a moderate selectivity index (SI ~ 1.0) for all the three tumoral cell lines investigated (Colo-205, NCI-H460 and U937).

While complexes (1) and (4) contains only the ligand HBPA (one and two, respectively), complex (2) has only the ligand HBHA (two molecules). On the other hand, complex (3) contains both ligands (one HBPA and one HBHA) (Scheme 1). From the biological point of view, the presence of both ligands (HBPA and HBHA) in the composition of (3) should result in a synergic effect. However, complex (3) was slightly less active than complex (4), and it was more toxic for PBMC than complexes (1) and (2). A positive feature of (3), in comparison to (4), is that (3) was twice less toxic to the normal cells than (4) (IC$_{50}$ = 36 ± 0.4 μM and 18 ± 0.5 μM, respectively). Such effect can be attributed to the presence of the ligand HBHA in (3), since complex (2), was the compound with the lowest cytotoxicity towards the normal cells (PBMC) (IC$_{50}$ = 82 ± 0.4 μM). Considering that complex (2) showed the lowest cytotoxicity to the normal cells and a satisfactory activity on lung cancer (NCI-H460) (IC$_{50}$ = 38 ± 0.5 μM), it was selected, together with (4), which showed the best activity, against all the tumoral cell lines under investigation (IC$_{50}$ = 20 ± 0.8, 25 ± 0.9 μM and 27 ± 0.1 μM, respectively) for the further studies.

Evaluation of the cell death pathway

According to the cell viability assay (Table 4), complexes (2) and (4) exhibited interesting cytotoxicity toward NCI-460, a cell culture resistant to cisplatin treatment (Sirichanchuen et al. 2012; Ballestreri et al. 2018). Complex (2) exhibited low cytotoxicity toward normal cells (PBMC) (IC$_{50}$ = 82 ± 0.4 μM), and complex (4) was very active towards all the tumoral cell lines. In order to determine the type of cell death induced by these complexes on NCI-H460 cells, the annexin V and propidium iodide (PI) staining study was carried out for 48 h (Fig. 5). In this type of experiment, normal cells are unmarked, cells in the early apoptosis stage are single marked with annexin V-labeled, late apoptosis cells (apoptosis–necrosis) are marked with both annexin V and PI and necrosis cells are PI-labeled only (Wlodkowic et al. 2011).

According to Fig. 5, 66% of NCI-H460 cells treated with 2 × IC$_{50}$ (76 μmol L^{-1}) of complex (2) were found in apoptosis. NCI-H460 cells treated with 2 × IC$_{50}$ (400 μmol L^{-1}) of cisplatin were mostly marked in the necrosis death quadrant under the same conditions (56%).

Since complex (4) was the most toxic towards the lung carcinoma cell (IC$_{50}$ = 25 ± 0.9 μM), its death mechanism was also investigated (Fig. 5). After 48 h incubation time with annexin V and propidium iodide complex (4) (2 × IC$_{50}$ = 50 μM) promoted 88% of cell death by apoptosis, being the best result observed for this experiment. On the other hand, cisplatin, in a concentration eight times higher than complex (4) (2 × IC$_{50}$ = 400 μM), promoted less than half of the apoptosis death percentage (39%). Only 9% of the remaining cells treated with complex (4) were marked in late apoptosis (apoptosis–necrosis).
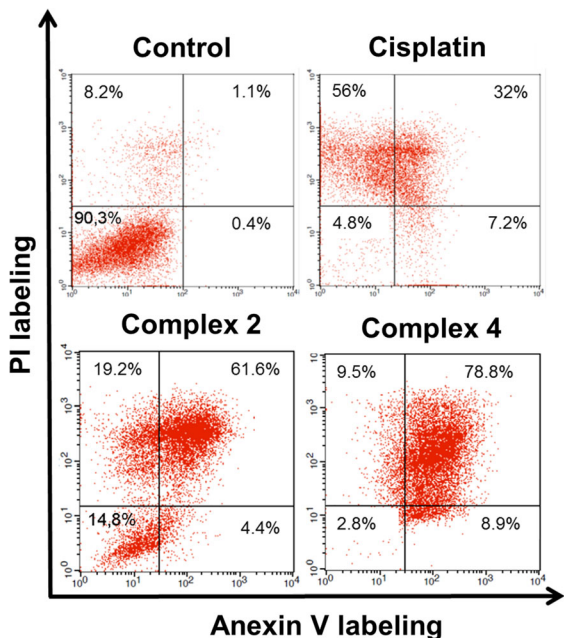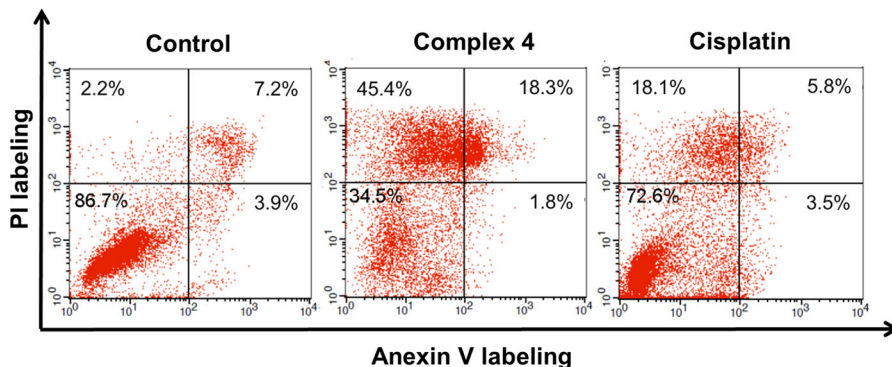
Fig. 5 Annexin V-FITC/PI staining of NCI-H460 cells after treatment for 48 h with complex (2), complex (4) and cisplatin
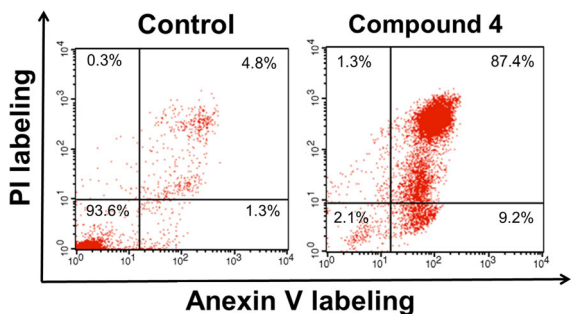
Fig. 6 Annexin V-FITC/PI staining of U-937 cells after treatment for 24 h with complex (4)

Fig. 7 Annexin V-FITC/PI staining of Colo-205 cells after treatment for 24 h with compound (4) and cisplatin

In order to verify the type of cell death induced by complex (4) against human monocyte lymphoma lineage (U937), annexin V and PI labeling was performed within 24 h. Complex (4) is very active toward this cell line ($IC_{50} = 27 \pm 0.1$ μM). About 97% of the cells treated with the complex (4) ($2 \times IC_{50} = 54$ μM) were unfeasible by apoptosis (Fig. 6). A similar study shows that the behavior of this complex is similar to the clinical drug cisplatin, inducing mainly apoptosis (96%) in this same cell line (Fernandes et al. 2015).

In the cell assay performed for Colo-205 during 24 h of incubation, using a cisplatin concentration of 260 μM ($2 \times IC_{50}$) approximately 73% of the cells remained viable and 18% were marked in necrosis. On the other hand, complex (4) at concentration of 40 μM ($2 \times IC_{50}$), promoted about 20% apoptosis cell death in this tumor line and 45% necrosis (Fig. 7).

Therefore, based on the results presented in Fig. 7, despite the interesting IC_{50} value presented by complex 4 towards Colo-205 cell line (20 ± 0.8 μM), after 24 h of incubation, the percentage of apoptosis is low (20%) and the necrosis one is considerably higher (about 45%). However, cisplatin does not promote expressive results, neither in apoptosis (only 10%) nor in necrosis (around 18%), probably due to its high IC_{50} value (> 100 μM). These results show that complex (2) promotes a high percentage of cell death by apoptosis towards NCI-H460 and U937 cell lines, and moderate percentage of necrosis toward Colo-205.

Conclusion

In this work, the successful synthesis of two new copper(II) complex obtained by the coordination of

the benzo hydroxamic acid (HBHA): [Cu(BHA)$_2$] (**2**) and [Cu(HBPA)(BHA)Cl] CH$_3$OH (**3**) was demonstrated. The reaction between complex (**1**) and HBHA resulted in the new complex (**3**), and its molecular structure was solved by X-ray diffraction. Complex (**2**) presents IC$_{50}$ values lower than cisplatin towards NCI-H460 (38 ± 0.5 μM and > 200 μM, respectively) and the best selectivity index obtained towards NCI-H460 (SI = 2.2) and U937 cell lines (SI = 2.0), as a result of the presence of two molecules of HBHA in its structure. Complex (**3**), which contains both ligands (HBPA and HBHA) in its structure, exhibits IC$_{50}$ values lower than cisplatin towards NCI-H460 (32 ± 0.2 μM and > 200 μM, respectively), Colo-205 (35 ± 0.2 μM and > 100 μM, respectively) and comparable results to cisplatin towards U937 (31 ± 0.9 μM and 20 ± 0.4 μM, respectively). Complex (**3**) shows higher cytotoxicity than complex (**2**), presenting a moderate selectivity index (SI ∼ 1.0) for all the three tumoral cell lines investigated (Colo-205, NCI-H460 and U-937). On the other hand, the insertion of a second HBPA ligand on the structure of complex (**1**) has resulted in [Cu(HBPA)$_2$]Cl$_2$· 4H$_2$O (**4**), which promoted major apoptosis death towards NCI-H460 and U-937 cells (88% and 97%, respectively) and 45% of death by necrosis toward Colo-205. In general, each ligand showed a distinct effect on the antitumoral activity, which was also related to the cell line investigated. HBHA ligand seems to lower the toxicity toward PBMC and HBPA is directly affecting the cytotoxity towards the tumoral cells investigated. These initial results highlight the improvements in the performance of the copper(II) complexes activity after the hydroxamic acid coordination, motivating us to carry future investigations.

Supplementary data

Crystallographic data (without structure factors) for the structure reported in this manuscript has been deposited with the Cambridge Crystallographic Data Centre as supplementary publication: deposition number: CCDC 2,008,656 for complex (**3**).

References

Addison AW, Rao TN, Reedijk J et al (1984) Synthesis, structure, and spectroscopic properties of copper(II) compounds containing nitrogen-sulphur donor ligands; the crystal and molecular structure of aqua[1,7-bis(N-methylbenzimidazol-2′;-yl)-2,6-dithiaheptane]copper(II) perchlorate. J Chem Soc Dalt Trans https://doi.org/10.1039/DT9840001349

Azeredo NFB, Bull ES, Resende JALC et al (2015) Crystal structure and behavior in solution of [Cu(HBPA)2]Cl2·4H2O [HBPA = (2-hydroxybenzyl-2-pyridyl-methyl)amine]. J Chem Crystallogr. https://doi.org/10.1007/s10870-015-0617-8

Ballestreri E, Simon D, de Souza AP et al (2018) Resistance mechanism to cisplatin in NCIH-460 non-small cell lung cancer cell line: investigating apoptosis, autophagy, and cytogenetic damage. Cancer Drug Resist. https://doi.org/10.20517/cdr.2017.02

Borges LJH, Bull ÉS, Fernandes C et al (2016) In vitro and in vivo studies of the antineoplastic activity of copper (II) compounds against human leukemia THP-1 and murine melanoma B16–F10 cell lines. Eur J Med Chem. https://doi.org/10.1016/j.ejmech.2016.07.018

Brabec V, Griffith DM, Kisova A et al (2012) Valuable insight into the anticancer activity of the platinum-histone deacetylase inhibitor conjugate, cis-[Pt(NH3)2malSAHA - 2H)]. Mol Pharm. https://doi.org/10.1021/mp300038f

BRUKER, APEX2 (2012) Bruker AXS Inc., Madison, WI, USA.

Codd R, Braich N, Liu J et al (2009) Zn(II)-dependent histone deacetylase inhibitors: Suberoylanilide hydroxamic acid and trichostatin A. Int J Biochem Cell Biol 41(736):739

Cooper AL, Greenberg VL, Lancaster PS et al (2007) In vitro and in vivo histone deacetylase inhibitor therapy with suberoylanilide hydroxamic acid (SAHA) and paclitaxel in ovarian cancer. Gynecol Oncol. https://doi.org/10.1016/j.ygyno.2006.09.011

Costa RO, Ferreira SS, Pereira CA et al (2018) A new mixed-valence Mn(II)Mn(III) compound with catalase and superoxide dismutase activities. Front Chem. https://doi.org/10.3389/fchem.2018.00491

Faggi E, Gavara R, Bolte M et al (2015) Copper(ii) complexes of macrocyclic and open-chain pseudopeptidic ligands: synthesis, characterization and interaction with dicarboxylates. Dalt Trans. https://doi.org/10.1039/c5dt01496d

Fernandes C, Horn A, Vieira-da-Motta O et al (2010) Synthesis, characterization and antibacterial activity of FeIII CoII, CuII and ZnII complexes probed by transmission electron microscopy. J Inorg Biochem. https://doi.org/10.1016/j.jinorgbio.2010.07.011

Fernandes C, Horn A, Vieira-Da-Motta O et al (2014) Synthesis, characterization, antibacterial and antitumoral activities of mononuclear zinc complexes containing tridentate amine based ligands with N3 or N2O donor groups. Inorganica Chim Acta. https://doi.org/10.1016/j.ica.2014.02.040

Fernandes C, Horn A, Lopes BF et al (2015) Induction of apoptosis in leukemia cell lines by new copper(II) complexes containing naphthyl groups via interaction with death receptors. J Inorg Biochem. https://doi.org/10.1016/j.jinorgbio.2015.09.014

Geary WJ (1971) The use of conductivity measurements in organic solvents for the characterisation of coordination compounds. Coord Chem Rev. https://doi.org/10.1016/S0010-8545(00)80009-0

Griffith DM, Duff B, Suponitsky KY et al (2011a) Novel trans-platinum complexes of the histone deacetylase inhibitor valproic acid; synthesis, in vitro cytotoxicity and mutagenicity. J Inorg Biochem. https://doi.org/10.1016/j.jinorgbio.2011.03.001

Griffith DM, Szocs B, Keogh T et al (2011b) Suberoylanilide hydroxamic acid, a potent histone deacetylase inhibitor; its X-ray crystal structure and solid state and solution studies of its Zn(II) Ni(II), Cu(II) and Fe(III) complexes. J Inorg Biochem. https://doi.org/10.1016/j.jinorgbio.2011.03.003

Gupta SP, Sharma A (2013) The chemistry of hydroxamic acids. In: Hydroxamic acids: a unique family of chemicals with multiple biological activities

Halaburková A, Jendželovský R, Kovaľ J et al (2017) Histone deacetylase inhibitors potentiate photodynamic therapy in colon cancer cells marked by chromatin-mediated epigenetic regulation of CDKN1A. Clin Epigenetics. https://doi.org/10.1186/s13148-017-0359-x

Hathaway BJ, Billing DE (1970) The electronic properties and stereochemistry of mono-nuclear complexes of the copper(II) ion. Coord Chem Rev. https://doi.org/10.1016/S0010-8545(00)80135-6

Kalfaolu E, Karabulut B (2011) Theoretical investigation of EPR and molecular orbital coefficient parameters for [Cu(hsm)2(sac)2] complex. Chem Phys Lett. https://doi.org/10.1016/j.cplett.2011.02.038

Kenny RG, Marmion CJ (2019) Toward multi-targeted platinum and ruthenium drugs—a new paradigm in cancer drug treatment regimens? Chem Rev 119.2:1058–1137

Kenny RG, Ude Z, Docherty JR, Marmion CJ (2020) Vorinostat and Belinostat, hydroxamate-based anti-cancer agents, are nitric oxide donors. J Inorg Biochem. https://doi.org/10.1016/j.jinorgbio.2019.110981

Kim MS, Blake M, Baek JH et al (2003) Inhibition of histone deacetylase increases cytotoxicity to anticancer drugs targeting DNA. Cancer Res 63(7291):7300

Kivelson D, Neman R (1961) ESR studies on the bonding in copper complexes. J Chem Phys doi. https://doi.org/10.1063/11731880

Kovacic P, Edwards CL (2011) Hydroxamic acids (therapeutics and mechanism): Chemistry, acyl nitroso, nitroxyl, reactive oxygen species, and cell signaling. J Recept Signal Transduct 31(10):19

Končić MZ, Barbarić M, Perković I, Zorc B (2011) Antiradical, chelating and antioxidant activities of hydroxamic acids and hydroxyureas. Molecules. https://doi.org/10.3390/molecules16086232

Luu TH, Morgan RJ, Leong L et al (2008) A phase II trial of vorinostat (suberoylanilide hydroxamic acid) in metastatic breast cancer: a California cancer consortium study. Clin Cancer Res. https://doi.org/10.1158/1078-0432.CCR-08-0122

Maciel LLF, de Freitas WR, Bull ES et al (2020) In vitro and in vivo anti-proliferative activity and ultrastructure investigations of a copper(II) complex toward human lung cancer cell NCI-H460. J Inorg Biochem. https://doi.org/10.1016/j.jinorgbio.2020.111166

Manal M, Chandrasekar MJN, Gomathi Priya J, Nanjan MJ (2016) Inhibitors of histone deacetylase as antitumor agents: a critical review. Bioorg Chem 67(18):42

Marks PA (2007) Discovery and development of SAHA as an anticancer agent. Oncogene 26(1351):1356

Marmion CJ, Parker JP, Nolan KB (2013) Hydroxamic acids: an important class of metalloenzyme inhibitors. In: Comprehensive inorganic chemistry II (second edition): from elements to applications

Maurice AM (1980) Acquisition of anisotropic information by computational analysis of isotropic EPR spectra. (PhD thesis). University of Illinois, Urbana.

Morcelli SR, Bull ÉS, Terra WS et al (2016) Synthesis, characterization and antitumoral activity of new cobalt(II)-complexes: effect of the ligand isomerism on the biological activity of the complexes. J Inorg Biochem. https://doi.org/10.1016/j.jinorgbio.2016.05.003

Moreira RO, Morcelli SR, Kanashiro MM et al (2019) Modulating the antitumoral activity by the design of new platinum(II) compounds: synthesis, characterization, DFT, ultrastructure and mechanistic studies. J Inorg Biochem. https://doi.org/10.1016/j.jinorgbio.2018.12.016

Muller PY, Milton MN (2012) The determination and interpretation of the therapeutic index in drug development. Nat Rev Drug Discov 11.10(751):761

Neves A, de Brito MA, Vencato I et al (1993) Synthesis, crystal structure and properties of a new binuclear iron(III) complex as a model for the purple acid phosphatases. Inorganica Chim Acta. https://doi.org/10.1016/S0020-1693(00)87516-7

Park S, Park JA, Kim YE et al (2015) Suberoylanilide hydroxamic acid induces ROS-mediated cleavage of HSP90 in leukemia cells. Cell Stress Chaperones. https://doi.org/10.1007/s12192-014-0533-4

Parker JP, Nimir H, Griffith DM et al (2013) A novel platinum complex of the histone deacetylase inhibitor belinostat: Rational design, development and in vitro cytotoxicity. J Inorg Biochem. https://doi.org/10.1016/j.jinorgbio.2013.03.011

Rieger AM, Nelson KL, Konowalchuk JD, Barreda DR (2011) Modified annexin V/propidium iodide apoptosis assay for accurate assessment of cell death. J Vis Exp. https://doi.org/10.3791/2597

Rodrigues DA, Ferreira-Silva GA, Ferreira ACS et al (2016) Design, synthesis, and pharmacological evaluation of novel n-acylhydrazone derivatives as potent histone deacetylase 6/8 dual inhibitors. J Med Chem. https://doi.org/10.1021/acs.jmedchem.5b01525

Saban N, Bujak M (2009) Hydroxyurea and hydroxamic acid derivatives as antitumor drugs. Cancer Chemother Pharmacol 64:213

Sheldrick GM (2008) A short history of SHELX. Acta Crystallogr Sect A Found Crystallogr 64:112

Silva GC, Parrilha GL, Carvalho NMF et al (2008) A bio-inspired Fe(III) complex and its use in the cyclohexane

oxidation. Catal Today. https://doi.org/10.1016/j.cattod.2007.12.036

Sirichanchuen B, Pengsuparp T, Chanvorachote P (2012) Long-term Cisplatin exposure impairs autophagy and causes cisplatin resistance in human lung cancer cells. Mol Cell Biochem. https://doi.org/10.1007/s11010-011-1199-1

Ungerstedt J, Du Y, Zhang H et al (2012) In vivo redox state of Human thioredoxin and redox shift by the histone deacetylase inhibitor suberoylanilide hydroxamic acid (SAHA). Free Radic Biol Med. https://doi.org/10.1016/j.freeradbiomed.2012.09.019

Wang XX, Wan RZ, Liu ZP (2018) Recent advances in the discovery of potent and selective HDAC6 inhibitors. Eur J Med Chem 143:1406–1418

Wlodkowic D, Telford W, Skommer J, Darzynkiewicz Z (2011) Apoptosis and beyond: cytometry in studies of programmed cell death a review on hydroxamic acids: widespectrum chemotherapeutic agents. Int J Biol Biomed Eng. https://doi.org/10.46300/91011.2020.14.12

Publisher's Note Springer Nature remains neutral with regard to jurisdictional claims in published maps and institutional affiliations.